

Precision limit under weak-coupling with ancillary qubit

Peng Chen¹ and Jun Jing^{1,*}

¹*School of Physics, Zhejiang University, Hangzhou 310027, Zhejiang, China*

We propose a measurement-based quantum metrology protocol in a composite model, where the probe system (a spin ensemble) is coupled to an ancillary two-level system (qubit) with a general Heisenberg XXZ interaction. With an optimized and weak probe-ancilla coupling strength and a proper duration of joint evolution, the two parallel evolution paths of the probe system induced by the unconditional measurement on qubit can transform an eigenstate of the collective angular momentum operator of spin ensemble to be a two-component state with a large distance in eigenspace. The quantum Fisher information about the phase encoded in the probe system of polarized states or their superposition, that could be relaxed to mixed states, can therefore manifest an exact or asymptotic quadratic scaling with respect to the probe size (spin number) N . The quadratic scaling behavior is found to be insensitive to the imperfect encoding operator and coupling strength. By virtue of the parity detection on the ancillary qubit or the probe system, the phase sensitivity can approach the Heisenberg limit. We suggest that the unconditional measurement on qubit could become an efficient resource to replace Greenberger-Horne-Zeilinger-like states and squeezing Hamiltonian for exceeding the standard quantum limit in metrology precision.

I. INTRODUCTION

Quantum metrology [1–6] is an emerging field that integrates quantum mechanics with statistics. It holds significant importance for a variety of quantum sciences and technologies, including atomic clock [7, 8], gravitational wave detection [9], biological sensing [10, 11], and magnetometry [12]. The general goal of quantum metrology is to achieve a high sensitivity in parameter estimation. A conventional quantum estimation protocol [1, 2, 4] consists of (1) preparing a probe into a resource state, (2) encoding the to-be-estimated parameter into the probe state, (3) performing certain measurements or detections on the probe system to extract parametric information, and (4) processing the detection outcomes to estimate the parametric precision. The precision of quantum metrology using uncorrelated probe states as input is bounded by the standard quantum limit (SQL), which scales as $1/\sqrt{N}$ with N the subunit number of the atomic probe systems or the number of measurements [13]. The quantum mechanics in metrology precision [14] is highlighted with the scaling advantage of the Heisenberg limit (HL) over SQL. It depends on resource states and presents a scaling law inverse to the system size N .

A common strategy to enhance metrology precision is the use of certain nonclassical states as resource states, including the many-body entangled states and squeezed spin states. Highly entangled states have been prepared and the Heisenberg limit is observed in small-scale systems [15–17]. For example, the size of Greenberger-Horne-Zeilinger (GHZ) states that can be generated on a quantum processor has reached 18 qubits, with a fidelity ~ 0.525 . However, the generation of GHZ states for a large atomic ensemble remains a significant challenge due to the high susceptibility to environmental de-

coherence. Squeezed spin states [2, 18, 19] are another widely explored class of nonclassical resources, which enhance the sensitivity of quantum measurements through suppressed quantum fluctuations. Also they are featured with a higher tolerance to decoherence and a lower loss than GHZ states [20]. Collective one-axis twisting (OAT) Hamiltonian $H_{\text{OAT}} = \chi J_z^2$ is widely applied to deterministically produce strong squeezing, which yields a sub-HL noise-reduction $\propto 1/N^{2/3}$ for N particles with the optimized duration $\chi t \simeq 3^{1/6} N^{-2/3}$ [18, 21]. The nonlinear atomic collisions in two-component Bose-Einstein condensate give rise to an OAT interaction [22–24]. In the systems of cavity quantum electrodynamics, the OAT Hamiltonian can be engineered via dispersive atom-light interaction [25–27], in which the atom-atom interaction is mediated by photons within the cavity. Other studies to produce OAT interaction use trapped ions [28–30] or lattice systems [31–33].

Exploring non-entangled probes in quantum metrology has gained considerable attentions in recent years, exemplified by the coupling or the entanglement between the probe and an ancillary system as an external resource for outperforming SQL in the parametric estimation [34–36] or increasing the protocol’s robustness against noise [37–42]. In a phase estimation protocol [36], the interaction between a photonic system and an ancillary qubit can be manipulated by an external field, enabling the photonic system to be transformed from the vacuum state into a NOON state. By performing measurements over the photon number, the phase precision can be enhanced to HL for the entire regime of the unknown parameter. In a protocol for measuring the frequency of identical probe units [34], the parameter information can be efficiently extracted via measurements on the ancillary qubit, after tracing out the probe system. By properly tailoring the interaction Hamiltonian, the time points for measurements, and the coupling strength, the estimation precision can reach the Heisenberg scaling at special periodic time points in terms of probe size.

* Contact author: jingjun@zju.edu.cn

The quantum metrologies assisted by the external interaction [34–36], however, demand the time-dependent and strong coupling strength or specific interaction Hamiltonian. For example, the time-reversal strategy [36], that is used to saturate the Cramér-Rao bound in phase estimation, requires a tunable transversal coupling strength g between probe modes and the ancillary qubit and the magnitude of g is in the same order as the qubit frequency ω_A . The protocol using the noncommutation relation between probe Hamiltonian and interaction Hamiltonian [34] is optimized when the coupling strength is equivalent to the to-be-estimated frequency of identical probe units, i.e., $g = \omega_P$. A weak-coupling protocol is therefore highly desired in reality, which is the first motivation of the current work.

In this paper, we propose a high-precision protocol based on a general Heisenberg XXZ interaction between the probe system (a spin ensemble) and the ancillary qubit. It does not require a strong or tunable coupling strength. The unconditional measurement on qubit can induce two parallel evolution paths of the probe system. When the strengths of the longitudinal and transversal interactions are close to each other, an eigenstate of the collective angular momentum operator of the probe system can then be transformed to a superposed state distributed with a large distance in eigenspace. If the probe is prepared as a polarized state along an optimized direction, it can evolve to a GHZ-like state after the unconditional measurement on qubit. An asymptotic Heisenberg-scaling behavior about the metrology precision can be obtained even when the probe is prepared as a thermal state. This asymptotic scaling behavior is insensitive to the imprecise direction about the phase encoding and the strengths along both transversal and longitudinal directions. To extract the information about the to-be-estimated parameter, we can perform the parity detections on either ancillary qubit or probe system, both of which approach HL in the phase sensitivity.

The rest of this work is structured as follows. Section II introduces the circuit model of our metrology protocol with the unconditional measurement on the ancillary qubit. In Sec. III, we study the conditions about the systematic parameters and the initial state of the probe system for attaining the Heisenberg limit. In Sec. IV, we discuss the sensitivity of our metrology protocol to the imprecise controls over the direction of the phase encoding and the coupling strengths. We analyze the phase sensitivity under parity detection performed on the ancillary qubit and the probe system in Secs. VA and VB, respectively. The entire work is summarized in Sec. VI. Appendix A provides a detailed derivation of the joint evolution operator for the full Hamiltonian.

II. MODEL AND HAMILTONIAN

Consider a quantum metrology model about a large-spin probe (spin ensemble) coupled to an ancillary spin-

1/2 (qubit) by a general Heisenberg XXZ interaction. The full Hamiltonian can be written as ($\hbar \equiv 1$)

$$H = \omega_P J_z + \omega_A \sigma_z + g_z J_z \sigma_z + g(J_x \sigma_x + J_y \sigma_y), \quad (1)$$

where $J_\mu = \sum_{l=1}^N \sigma_\mu^l / 2$, $\mu = x, y, z$, represents the collective spin operator with N the total spin number of the probe ensemble and σ_μ^l the μ -component of Pauli operator for the l th probe spin. $\sigma_{x,y,z}$ is the Pauli matrix of the ancillary qubit. ω_P and ω_A denote the energy splitting of the probe spin and the ancillary spin, respectively. g and g_z denote the transversal and longitudinal coupling strengths, respectively.

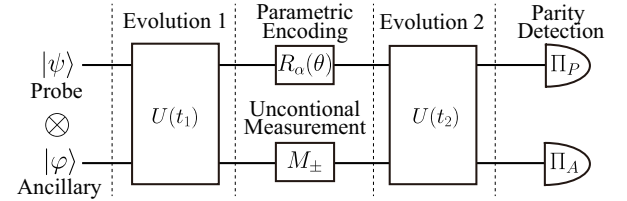


FIG. 1. A circuit model of our measurement-based metrology. The composite system prepared in a separable state $|\psi\rangle \otimes |\varphi\rangle$ experiences two stages of free joint unitary evolutions $U(t_1)$ and $U(t_2)$. In between them, a to-be-estimated phase parameter θ is encoded into the large-spin-probe system via a unitary rotation $R_\alpha(\theta)$ on the equatorial plane and meanwhile an unconditional measurement $M_\pm = |\pm\rangle\langle\pm|$ in the basis of σ_x is performed on the ancillary qubit. The output state is determined by the parity detections on the probe system or the ancillary qubit.

The Heisenberg XXZ interaction in Eq. (1) is popular in various experimental platforms. In nitrogen-vacancy (NV) center systems [43], J_μ describes the ^{15}N nuclear spins and σ_μ describes the NV electron spin consisting of $m_s = 0, 1$ that is isolated by applying a magnetic field parallel to the quantization axis of the NV center. Under the external magnetic field $B = 10^3$ G, the probe-spin frequency is about 108 MHz, the ancillary-spin frequency is about 60 MHz, and their coupling strengths g_z and g are found to be about 2.30 MHz and 2.10 MHz [44], respectively. In quantum-dot systems [45, 46], J_μ and σ_μ describe the nuclear spins and the electron spin, respectively. The probe frequency is about $\omega_P = 5$ MHz, the ancillary frequency is about $\omega_A = 2.5$ GHz, and the coupling strengths $g_z \approx g \approx 80$ MHz, under the external magnetic field $B = 379$ G. It turns out that (i) the coupling strengths are much weaker than the system frequency and (ii) the longitudinal coupling strength is usually close to the transversal one. Our metrology method can be practiced in these systems, since the Heisenberg scaling in metrology precision can be achieved as long as $\sqrt{g_z^2 - g^2} = (2\omega_A - \omega_P)/(N + 1)$ [see Eq. (9a)].

As shown in Fig. 1, the probe spin ensemble and the ancillary qubit are assumed to be initially separable, i.e., the input state of the composite system is a product state $|\psi\rangle \otimes |\varphi\rangle$. The nonunitary evolution operator for the

entire circuit can be written as

$$U_{\theta,\pm} = U(t_2)R_\alpha(\theta)M_\pm U(t_1) \\ = e^{-iHt_2}e^{-i\theta J_\alpha}|\pm\rangle\langle\pm|e^{-iHt_1}, \quad (2)$$

where t_1 and t_2 are the durations of the two stages of joint unitary evolution, respectively, and $|\pm\rangle \equiv (|e\rangle \pm |g\rangle)/\sqrt{2}$ are the eigenbases of σ_x with $|g\rangle$ and $|e\rangle$ being the ground and excited states of the ancillary qubit. The spin rotation $R_\alpha(\theta) = \exp(-i\theta J_\alpha)$ describes the parametric encoding into the probe spin system, where $J_\alpha = \cos\alpha J_x + \sin\alpha J_y$ is a general collective angular momentum operator lying in the x - y equatorial plane of the Bloch sphere, oriented at an arbitrary angle α with respect to the x axis. The spin rotation around an arbitrary direction could be practiced by a sequence of rotations $R_\alpha(\theta) = R_z(\alpha)R_y(\pi/2)R_z(\theta)R_y(-\pi/2)R_z(-\alpha)$, where $R_z(\pm\alpha)$ and $R_y(\pm\pi/2)$ indicate α and $\pi/2$ pulses applied along the z and y axes, respectively, and $R_z(\theta)$ could be generated by a dispersive coupling between the probe system and a to-be-measured system [23, 47, 48]. Without loss of generality, J_α is assumed to be polarized along the x axis, such that $J_\alpha = J_x$ and $R_\alpha(\theta) = R_x(\theta)$ in Eq. (2). The projection operator $M_\pm \equiv |\pm\rangle\langle\pm|$ describes the unconditional measurement on the ancillary qubit. “Unconditional” means the whole process continues irrespective to the measurement outcome that would not be recorded. In experiments, the measurement over the ancillary qubit, e.g., the electron spin in NV center, can be realized by the collected fluorescence [49]. At the end of the entire circuit, a parity detection will be performed on either ancillary qubit or probe system (see Sec. V). The output signal and its fluctuation can be used to infer the phase sensitivity about the unknown θ .

III. QUANTUM FISHER INFORMATION OF THE MEASUREMENT-BASED METROLOGY

Previous works [14, 50] show that the quantum Fisher information associated with the phase to be estimated can be written as the variance of a phase generator with respect to the probe state. They indicate that the maximum QFI is attained when the probe is prepared in an equal superposition of the eigenstates with the maximum and minimum eigenvalues of the phase generator, such as the GHZ state in atomic systems or the NOON state in photonic systems. For a phase generator J_x of our large-spin system, the relevant GHZ-like state takes the form

$$|\text{GHZ}\rangle = \frac{1}{\sqrt{2}} (|j, \pm j\rangle_x + e^{-i\phi} |j, \mp j\rangle_x) \\ = \frac{1}{\sqrt{2}} (\mathcal{I}^{N+1} + e^{-i\phi} e^{-i\pi J_z}) |j, \pm j\rangle_x, \quad (3)$$

where $j = N/2$ is the quantum number with N the size of the probe spin ensemble, \mathcal{I}^{N+1} is the identity matrix of $N+1$ dimensions, ϕ is a local phase, and $|j, m\rangle_x$ is the eigenstate of the collective spin operators J_x with

eigenvalue m for $-j \leq m \leq j$. Here we have applied $|j, \mp j\rangle_x = e^{-i\pi J_z} |j, \pm j\rangle_x$ in the second line. GHZ state can be prepared by allowing the polarized state $|j, \pm j\rangle_x$ to undergo a two-path evolution, i.e., \mathcal{I}^{N+1} and $e^{-i\pi J_z}$, a possible strategy for which is indefinite gate order or dynamics [51–53]. For example, in a protocol about estimating the expectation-value product of position and momentum displacements of a continuous-variable system [51], an ancillary two-level system acts as a quantum SWITCH, creating a superposition of two paths. Along one path, all the position-displacement operators are performed before all the momentum-displacement operators; and along another one, the order is inverted. The estimation precision can therefore be enhanced up to the super-Heisenberg scaling in terms of the repetition number of position or momentum displacements.

In the circuit of Fig. 1, our protocol employs the free joint unitary evolution for Evolution 1 and the unconditional measurement M_\pm to construct the two-path evolution. Distinct measurement outcome about the ancillary qubit indicates distinct path of output. Despite we actually obtain a classical mixture of two paths on different outcomes, it is shown that the probability of one path can become ignorable as long as N is sufficiently large. Suppose the initial state of the qubit is $|\varphi\rangle = |+\rangle$ and according to Eq. (2), the unnormalized output state of the composite system then reads

$$|\Psi_\pm\rangle = M_\pm U(t_1)|\psi\rangle \otimes |\varphi\rangle = \langle \pm |U(t_1)|+\rangle |\psi\rangle \otimes |\pm\rangle, \quad (4)$$

with a probability $\mathcal{N}_\pm = \langle \Psi_\pm | \Psi_\pm \rangle$ after the first-stage evolution $U(t_1)$ and a measurement on qubit in its σ_x basis. Here the subscript indicates the measurement outcome. In particular, we have

$$|\Psi_+\rangle = \langle + |U(t_1)|+\rangle |\psi\rangle \otimes |+\rangle \\ = \frac{O_- + e^{-2i\Omega(J_z)t_1} O_+}{4} e^{i[\Omega(J_z) - A(J_z)]t_1} |\psi\rangle \otimes |+\rangle, \quad (5)$$

with the operator

$$O_\pm = 1 \pm \frac{\Lambda(J_z)}{\Omega(J_z)} \\ + e^{i\omega_P t_1} e^{\pm i[\Omega(J_z) - \Omega(J_z-1)]t_1} \left[1 \pm \frac{\Lambda(J_z-1)}{\Omega(J_z-1)} \right] \\ \pm e^{i\omega_P t_1} e^{i[\Omega(J_z) - \Omega(J_z+1)]t_1} \frac{g}{\Omega(J_z)} J_- \pm J_+ \frac{g}{\Omega(J_z)}, \quad (6)$$

where the operator functions are defined as

$$\omega(J_z) \equiv g\sqrt{(j - J_z)(j + J_z + 1)}. \quad (7a)$$

$$\Lambda(J_z) \equiv g_z \left(J_z + \frac{1}{2} \right) + \Delta_A, \quad (7b)$$

$$\Omega(J_z) \equiv \sqrt{\omega^2(J_z) + \Lambda^2(J_z)}. \quad (7c)$$

$$A(J_z) \equiv \omega_P \left(J_z + \frac{1}{2} \right) - \frac{g_z}{2}, \quad (7d)$$

Here $\Delta_A \equiv \omega_A - \omega_P/2$ is the detuning between the ancillary qubit and the probe spin. The derivation details of

the free joint evolution operator $U(t)$ for the full Hamiltonian (1) is provided in Appendix A. It is found that when

$$e^{-2i\Omega(J_z)t_1} = e^{-i\phi}e^{-i\pi J_z}, \quad (8a)$$

$$|\langle j, \pm j |_x (O_- + O_+) e^{i[\Omega(J_z) - A(J_z)]t_1} |\psi\rangle| = 4\sqrt{2\mathcal{N}_+}, \quad (8b)$$

the probe state $|\Psi_+\rangle$ in Eq. (5) becomes the same as the GHZ-like state in Eq. (3) up to a global phase. In this case, $|\Psi_+\rangle$ is a superposition of two parallel evolution paths respectively indicated by \mathcal{I}^{N+1} and $e^{-2i\Omega(J_z)t_1}$.

With Eqs. (7a), (7b), and (7c), the solutions to Eq. (8a) can be found as

$$\sqrt{g_z^2 - g^2} = \frac{2\Delta_A}{N+1}, \quad (9a)$$

$$t_1 = t_{1,\text{opt}}(n_1) \equiv \frac{(N+1)(2n_1+1)}{4} \frac{\pi}{\Delta_A}, \quad (9b)$$

where n_1 is an integer. Equation (9a) suggests that the transversal coupling strength in our protocol should not be larger than the longitudinal coupling strength and our interaction Hamiltonian could be reduced to ZZ coupling between probe and ancillary system. Consequently, the phase parameter ϕ in Eq. (8a) reads,

$$\phi = (2n_1+1) \left[\frac{1}{2} + (N+1)^2 \frac{g_z}{4\Delta_A} \right] \pi. \quad (10)$$

In the large-number limit of N , we have $g \approx g_z$ and hence $\Lambda(J_z)/\Omega(J_z) \approx (2J_z+1)/(N+1)$, $g_{J+}/\Omega(J_z) \approx 2J_+/(N+1)$, according to Eqs. (9a), (7b), and (7a). Subsequently, a proper probe state

$$|\psi\rangle = |j, \pm j\rangle_{\text{opt}} = e^{-i[\Omega(J_z) - A(J_z)]t_{1,\text{opt}}} |j, \pm j\rangle_x \quad (11)$$

and a proper eigenfrequency

$$\omega_P = \frac{n_P}{t_{1,\text{opt}}} \pi \quad (12)$$

with n_P integer constitute a solution to Eq. (8b). Here $|j, m\rangle_{\text{opt}}$'s with $-j \leq m \leq j$ denote the eigenstates for the optimized collective angular momentum operator

$$\begin{aligned} J_{\text{opt}} &= e^{-i[\Omega(J_z) - A(J_z)]t_{1,\text{opt}}} J_x e^{i[\Omega(J_z) - A(J_z)]t_{1,\text{opt}}} \\ &= (-1)^{(n_P+1)} J_y. \end{aligned} \quad (13)$$

Using one of the optimized probe states in Eq. (11) $|\psi\rangle = |j, -j\rangle_{\text{opt}}$ and the conditions in Eqs. (9a), (9b), and (12), the unnormalized output state of the composite system under the entire circuit of evolution in Eq. (2) can be expressed as

$$\begin{aligned} |\Psi_{\theta,\pm}\rangle &\approx \frac{1 \mp i(-1)^{n_1+n_P}}{4(N+1)} U(t_2) R_x(\theta) \\ &\quad \left\{ [(N \mp 2J_x) \pm 2i(-1)^{n_1+n_P} J_{\mp,x}] \right. \\ &\quad \left. \pm i(-1)^{n_1(N+1)+n_P} e^{-i\phi} e^{-i\pi J_z} \right. \\ &\quad \left. [(N+2 \mp 2J_x) \pm 2i(-1)^{n_1+n_P} J_{\pm,x}] \right\} \\ &|j, -j\rangle_x \otimes |\pm\rangle, \end{aligned} \quad (14)$$

where $J_{\pm,x} \equiv -J_z \pm iJ_y$. The relevant probability reads

$$\mathcal{N}_{\theta,\pm} = \langle \Psi_{\theta,\pm} | \Psi_{\theta,\pm} \rangle = \frac{1}{2} \left(1 \pm \frac{N}{N+1} \right). \quad (15)$$

When $N \gg 1$, we have $\mathcal{N}_{\theta,+} \rightarrow 1$ and $\mathcal{N}_{\theta,-} \rightarrow 0$, indicating that the measurement result about the ancillary qubit is almost definitely $|+\rangle$. For either measurement result, the effective QFI is defined as

$$F_{Q,\pm} = 4\mathcal{N}_{\theta,\pm} [\langle \partial_\theta \Psi'_{\theta,\pm} | \partial_\theta \Psi'_{\theta,\pm} \rangle - |\langle \Psi'_{\theta,\pm} | \partial_\theta \Psi'_{\theta,\pm} \rangle|^2], \quad (16)$$

where the normalized state is $|\Psi'_{\theta,\pm}\rangle = |\Psi_{\theta,\pm}\rangle / \sqrt{\mathcal{N}_{\theta,\pm}}$. Thus, the full QFI reads

$$F_Q = F_{Q,+} + F_{Q,-} \approx N^2 \left[1 - \frac{4}{(N+1)^2} \right]. \quad (17)$$

Then for a large-size probe, i.e., $N \gg 1$, the quantum Fisher information can be approximated as $F_Q \approx N^2$.

When the probe system is prepared in another optimized state $|\psi\rangle = |j, j\rangle_{\text{opt}}$ in Eq. (11), one can obtain an unnormalized output state similar to Eq. (14) under the optimal conditions in Eqs. (9a), (9b), and (12). The relevant probability in Eq. (15) now becomes $\mathcal{N}_{\theta,\pm} = [1 \mp N/(N+1)]/2$. It means that the ancillary qubit after the unconditional measurement is almost certainly found in the state $|-\rangle$ under the large- N limit. Consequently, one can obtain the same result as Eq. (17).

The preceding analysis demonstrates that the Heisenberg scaling in metrology precision can be approached when the probe and the ancillary qubit are prepared at a proper state $|\psi\rangle$ in Eq. (11) and $|\varphi\rangle = |+\rangle$, respectively, and the joint evolution time is scheduled as t_1 in Eq. (9b) before encoding in probe and measurement on qubit. Similarly, if the ancillary qubit is initialized as $|\varphi\rangle = |-\rangle$, one can obtain the same sufficient conditions in Eqs. (8a) and (8b) or Eqs. (9a), (9b), (11), and (12) under the large- N limit for generating the GHZ-like state. QFI also shows the same scaling behavior as in Eq. (17). In the following, we then always assume $|\varphi\rangle = |+\rangle$ and $|\psi\rangle = |j, -j\rangle_{\text{opt}}$.

Next, we consider a more general case, where the probe system is prepared as a pure state superposed by the eigenbases of the specific optimized collective angular momentum operator in Eq. (13), e.g., $|\psi_m\rangle = a_m |j, m\rangle_{\text{opt}} + b_m e^{-i\phi_m} |j, -m\rangle_{\text{opt}}$ with $1 \leq m \leq j$ and real numbers a_m , b_m , and ϕ_m . Upon the preceding optimal conditions in Eqs. (9a), (9b), and (12), one can still obtain a square-scaling QFI:

$$\begin{aligned} F_Q &\approx 4 \left[1 - \frac{6}{(N+1)^2} \right] m^2 - \frac{[(N+1)^2 - 4m^2]^2}{(N+1)^2 - 4m^2(a_m^2 - b_m^2)^2} \\ &\quad \times \frac{16m^2}{(N+1)^2} a_m^2 b_m^2 \sin^2 \phi_m \sin^2 \left(\phi + \frac{N+1}{2} \pi \right) \\ &\quad + (-1)^N 8m \frac{N(N+2) - 4m^2}{(N+1)^2} a_m b_m \\ &\quad \times \sin \phi_m \sin \left(\phi + \frac{N+1}{2} \pi \right) + \frac{2N^2}{(N+1)^2} \end{aligned} \quad (18)$$

up to the order of N^0 . Given a quantum number m , QFI can be approximated as $F_Q \approx 4[1 - 6/(N+1)^2]m^2 + 2N^2/(N+1)^2$, which reduces to Eq. (17) for $m = j$, by eliminating the second term in Eq. (18). It occurs under any of the following conditions: (i) $a_m b_m = 0$, (ii) $\phi_m = n_m \pi$, or (iii) $\phi + (N+1)\pi/2 = n_\phi \pi$, with n_m and n_ϕ integers. Here the first two conditions correspond to optimizing the input state, or more precisely, the population distribution and the relative phase ϕ_m of the probe system. The last one, i.e., $\phi + (N+1)\pi/2 = n_\phi \pi$, depends only on the ratio of the systematic parameters g_z/Δ_A in Eq. (10), which is equivalent to require

$$g_z = \frac{N+2n_\phi-2}{2n_1+1} \frac{2\Delta_A}{(N+1)^2}. \quad (19)$$

Here we have used the optimized joint evolution time $t_{1,\text{opt}}$ in Eq. (9b). Equation (18) therefore confirms that the polarized states $|j, \pm j\rangle_{\text{opt}}$ in Eq. (11) can be regarded as efficient resources to replace the standard GHZ-like states for approaching HL in metrology precision.

An asymptotic Heisenberg-scaling behavior of QFI can however appear even when the probe state is prepared as a mixed state. For example, one can suppose that the probe system is prepared as a thermal state in the bases of the optimized collective angular momentum operator J_{opt} in Eq. (13). We then have

$$\rho_P^{\text{th}} = \sum_{m=-j}^j \frac{e^{-m\beta}}{Z_\beta} |j, m\rangle_{\text{opt}} \langle j, m|, \quad (20)$$

where $Z_\beta = \text{Tr}[\exp(-\beta J_{\text{opt}})]$ is the partition function and $\beta \equiv \omega_P/(k_B T)$ is the dimensionless inverse temperature. Using Eqs. (2), the unnormalized output state after the whole evolution operator can be written as

$$\rho(\theta) = U_{\theta,+} \rho_P^{\text{th}} \otimes \rho_A U_{\theta,+}^\dagger + U_{\theta,-} \rho_P^{\text{th}} \otimes \rho_A U_{\theta,-}^\dagger, \quad (21)$$

where the first and second terms correspond to the measurement results $|+\rangle$ and $|-\rangle$ about the ancillary qubit with probabilities $\mathcal{N}_\pm = \text{Tr}[U_{\theta,\pm} \rho_P^{\text{th}} \otimes \rho_A U_{\theta,\pm}^\dagger]$, respectively, and ρ_A is the initial state of ancillary qubit.

In the low-temperature regime, the population of the probe system is mostly on the ground state $|j, -j\rangle_{\text{opt}}$. According to Eq. (15), $\mathcal{N}_+ \approx \mathcal{N}_{\theta,+} \rightarrow 1$ in the large- N limit. Thus, we can only consider the measurement outcome $|+\rangle$, i.e., $\rho(\theta) \approx U_{\theta,+} \rho_P^{\text{th}} \otimes \rho_A U_{\theta,+}^\dagger$. Using the optimized conditions in Eqs. (9a), (9b), (11), and (12) and $\rho_A = |+\rangle\langle +|$, the normalized output state can be approximately derived as

$$\begin{aligned} \rho(\theta) &\approx \mathcal{N}_+^{-1} U_{\theta,+} \rho_P^{\text{th}} \otimes \rho_A U_{\theta,+}^\dagger \\ &\approx \sum_{m=-j}^j \left(\frac{N-2m}{4N} \right)^2 \frac{e^{-m\beta}}{Z_\beta \mathcal{N}_+} U'_\theta |j, m\rangle_{\text{opt}} \langle j, m| U'_\theta^\dagger \\ &\otimes |+\rangle\langle +|, \end{aligned} \quad (22)$$

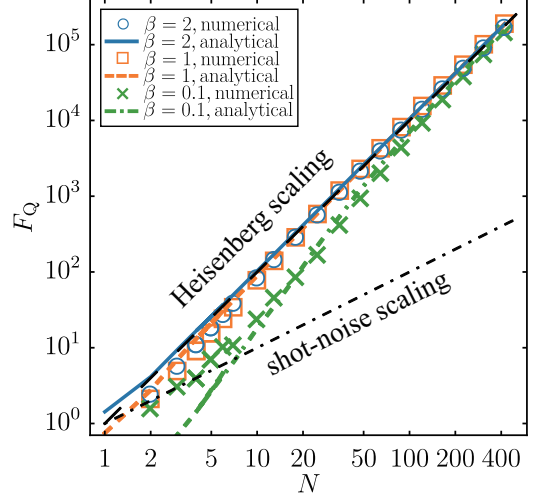


FIG. 2. QFI as a function of N for a thermal state ρ_P^{th} with various inverse temperatures. The black-dashed line and the black dot-dashed line indicate the Heisenberg and shot-noise scalings, respectively. Here $\rho_A = |\phi\rangle\langle\phi| = |+\rangle\langle +|$, $t_1 = (N+1)\pi/(4\Delta_A)$, $\omega_P/\Delta_A = 40/(N+1)$, $g_z/\Delta_A \approx 6/N$, and $g/\Delta_A \approx 4\sqrt{2}/N$.

where we have omitted the contribution from the raising and lowering operators $J_{\pm,x}$ in Eq. (14) and then the effective evolution operator turns out to be

$$U'_\theta = \frac{1 - i(-1)^{n_P}}{2} U(t_2) R_x(\theta) \times [1 + i(-1)^{n_1(N+1)+n_P} e^{-i\phi} e^{-i\pi J_z}]. \quad (23)$$

To have a unitary operator U'_θ , it is required that

$$U'_\theta^\dagger U'_\theta = 1 + \frac{i(-1)^{n_1(N+1)+n_P}}{2} \times (e^{-i\phi} e^{-i\pi J_z} - e^{i\phi} e^{i\pi J_z}) = \mathcal{I}^{N+1}, \quad (24)$$

which is equivalent to specialize the longitudinal coupling strength:

$$g_z = \frac{N+2n_z-1}{2n_1+1} \frac{2\Delta_A}{(N+1)^2} \quad (25)$$

with n_z integer. Together with the optimized conditions in Eq. (9a), QFI for the thermal state [54] can be written in a compact form

$$\begin{aligned} F_Q &= \sum_{m=-j}^j 4p_m \langle j, m | J_x^2 | j, m \rangle_{\text{opt}} \\ &- \sum_{m, m'=-j}^j \frac{8p_m p_{m'}}{p_m + p_{m'}} |\langle j, m | e^{-i\pi J_z} J_x | j, m' \rangle_{\text{opt}}|^2 \\ &= \frac{4}{\mathcal{N}_+} \sum_{m=-j}^j m^2 \left(\frac{N-2m}{4N} \right)^2 \frac{e^{-m\beta}}{Z_\beta} \\ &- \frac{8}{Z_\beta \mathcal{N}_+} \sum_{m=-j}^j \left(\frac{N-2m}{4N} \right)^2 \frac{m^2}{e^{-m\beta} + e^{m\beta}}, \end{aligned} \quad (26)$$

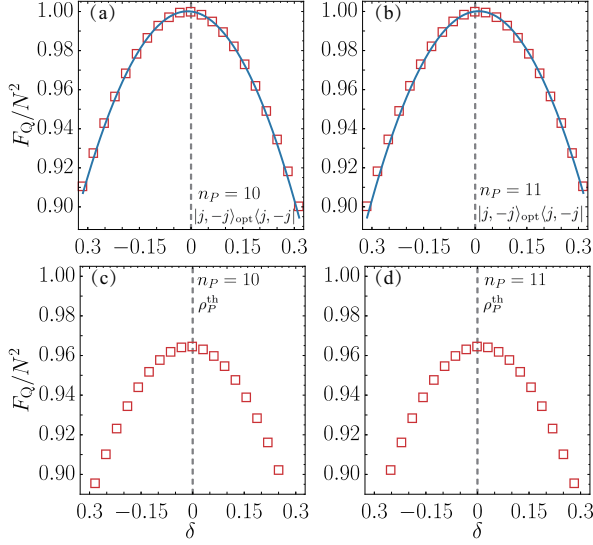


FIG. 3. Renormalized QFI F_Q/N^2 as a function of the deviation δ about encoding direction for the probe system prepared as (a) and (b) a polarized state $|\psi\rangle = |j, -j\rangle_{\text{opt}}$ or (c) and (d) a thermal state ρ_P^{th} with $\beta = 1$. The solid lines in (a) and (b) indicate the approximated analytical result in Eq. (29). The probe eigenfrequency ω_P is optimized by Eq. (12) with (a) and (c) an even number $n_P = 10$ and (b) and (d) an odd number $n_P = 11$. The probe size is $N = 100$. $t_1 = (N+1)\pi/(4\Delta_A)$, $g_z/\Delta_A \approx 6/N$, and $g/\Delta_A \approx 4\sqrt{2}/N$.

where $p_m = e^{-m\beta}(N-2m)^2/(16Z_\beta\mathcal{N}_+N^2)$.

The analytical result in Eq. (26), which holds the square scaling law of N under the large- N and low temperature limit, can be justified by the numerical simulation in Fig. 2 about QFI as a function of system size N for the thermal state ρ_P^{th} under various inverse temperatures. Without loss of generality, we choose $n_1 = 0$ in Eq. (9b), $n_P = 10$ in Eq. (12), and $n_z = N$ in Eq. (25), which yield $t_1 = (N+1)\pi/(4\Delta_A)$, $\omega_P/\Delta_A = 40/(N+1)$, and $g_z/\Delta_A = 2(3N-1)/(N+1)^2 \approx 6/N$, respectively. Subsequently, we have $g/\Delta_A = 4\sqrt{2N(N-1)/(N+1)^2} \approx 4\sqrt{2}/N$ according to Eqs. (9a). It is shown that a larger β yields a behavior closer to the Heisenberg scaling. The numerical results become indistinguishable from the approximate analytical results for $N \geq 10$, $N \geq 15$, and $N \geq 70$, when $\beta = 2$, $\beta = 1$, and $\beta = 0.1$, respectively. Even in case of $\beta = 0.1$, i.e., a high-temperature probe state, the scaling behavior of QFI approaches the Heisenberg limit for $N > 200$.

IV. EFFECTS OF IMPRECISE CONTROL

It is generally difficult to control both encoding process associated with the to-be-estimated phase and to-be-optimized protocol parameters with an infinite accuracy. Our protocol is confirmed to be robust against the small deviation of the direction of the phase encoding in Eq. (2) and the coupling strengths of both transversal

and longitudinal interactions in Eq. (9a).

In Eq. (2), we have set $\alpha = x$ for the direction of phase encoding. With a small angle deviation from the x axis, denoted by δ , the encoding operator becomes

$$R'_x(\theta) = e^{-i\theta(J_x \cos \delta + J_y \sin \delta)} \approx e^{-i\theta[(1-\delta^2/2)J_x + \delta J_y]} \quad (27)$$

up to the second order of δ . With the ancillary qubit $|\varphi\rangle = |+\rangle$ and the optimal conditions of the probe state and the joint-evolution time in Eqs. (11) and (9b), the unnormalized output state in Eq. (14) becomes

$$\begin{aligned} |\Psi_{\theta, \pm}\rangle \approx & \frac{1 \mp i(-1)^{n_1+n_P}}{4(N+1)} U(t_2) R'_x(\theta) \\ & \{ [(N \mp 2J_x) \pm 2i(-1)^{n_1+n_P} J_{\mp, x}] \\ & \pm i(-1)^{n_1(N+1)+n_P} e^{-i\phi} e^{-i\pi J_z} \\ & [(N + 2 \mp 2J_x) \pm 2i(-1)^{n_1+n_P} J_{\pm, x}] \} \\ & |j, -j\rangle_x \otimes |\pm\rangle, \end{aligned} \quad (28)$$

The relevant probability $\mathcal{N}_{\theta, \pm}$ is still given by Eq. (15). Using Eqs. (16) and (17), the full quantum Fisher information under the large- N limit reads,

$$F_Q \approx \frac{N^2}{(N+1)^2} [(N+1)^2 - 4 - \delta(-1)^{n_P}(2N-1) - \delta^2(N^2+2N-2)] \quad (29)$$

up to the second order of δ . Determined by $dF_Q/d\delta = 0$, the maximum value of QFI is obtained when $\delta = (-1)^{n_P+1}(2N-1)/2(N^2+2N-2)$, which is sufficiently close to $\delta = 0$ for a large N . The parity of the integer n_P implies the optimal point of the deviation δ as well as the sign of the optimal δ .

Figures 3(a) and (b) demonstrate the dependence of QFI on the angle deviation δ under different parity of n_P for a probe ensemble with a moderate size of $N = 100$ prepared as the polarized state $|\psi\rangle = |j, -j\rangle_{\text{opt}}$. Due to Eq. (12), they have different ω_P that is determined by n_P . The other parameters, including t_1 , g_z , and g , are chosen the same as Fig. 2. As expected from Eq. (29), QFI takes the peak value nearly N^2 around $\delta = 0$ and exhibits an approximately symmetric distribution with a small right (left) shift for odd (even) n_P . For either n_P , QFI is insensitive to the angle deviation. F_Q/N^2 is found to be larger than 0.988 even when $|\delta| = 0.1$. Such an asymptotic Heisenberg-scaling behavior of QFI and its insensitivity to the imperfect encoding direction hold when the probe system starts from a mixed state. In Figs. 3(c) and (d), we choose the thermal state in Eq. (20) with $\beta = 1$. It is found that $F_Q/N^2 \approx 0.964$ at $\delta \approx \mp 0.01$ for even and odd n_P , respectively. And when $|\delta| = 0.1$, it is still larger than $F_Q/N^2 \approx 0.956$.

All the preceding calculations of QFI are performed under the optimized condition about both transversal and longitudinal coupling strengths as given by Eq. (9a). In Fig. 4, we simulate the renormalized QFI F_Q/N^2 in a wide regime of both g and g_z to show the impact

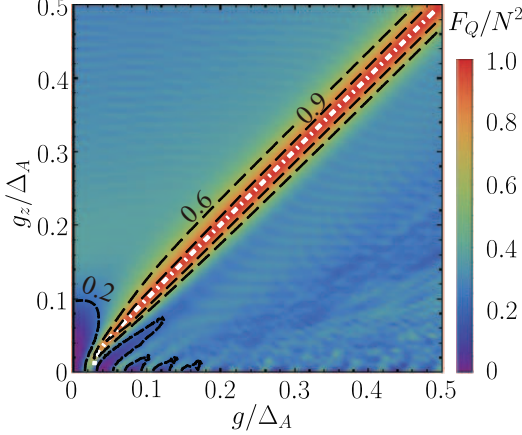


FIG. 4. Renormalized QFI F_Q/N^2 in the parametric space of g/Δ_A and g_z/Δ_A for the probe system prepared as the polarized state $|\psi\rangle = |j, -j\rangle_{\text{opt}}$ with the probe spin number $N = 100$. The white dot-dashed line presents the analytical result under the condition in Eq. (9a). Here $t_1 = t_{1,\text{opt}}(n_1 = 0) = (N + 1)\pi/(4\Delta_A)$.

from the imprecise control over the protocol parameters, where the probe system is initialized as the polarized state $|\psi\rangle = |j, -j\rangle_{\text{opt}}$ with $N = 100$ and the joint-evolution duration of the first stage is optimized as $t_1 = t_{1,\text{opt}}(n_1 = 0) = (N + 1)\pi/(4\Delta_A)$ as before. The white dot-dashed line indicates QFI of the maximum value N^2 obtained by the optimized coupling strengths satisfying Eq. (9a). The black dashed lines are the contour lines, by which one can find that the asymptotic quadratic scaling behavior of QFI remains valid when the probe-ancilla coupling strengths deviate from their optimal values with a certain magnitude. In particular, when the transversal coupling strength is fixed, e.g., $g/\Delta_A = 0.2$ and 0.4 , we have $F_Q/N^2 \geq 0.9$ in the regimes $0.19 \leq g_z/\Delta_A \leq 0.21$ and $0.39 \leq g_z/\Delta_A \leq 0.41$, respectively. When the transversal and longitudinal coupling strengths are balanced, e.g., $g_z/\Delta_A = g/\Delta_A \approx 0.043$ and 0.24 , we have $F_Q/N^2 \approx 0.84$ and 0.98 , respectively.

V. PHASE SENSITIVITY BASED ON PARITY DETECTION

In a practical scenario, it is important to quantify the ultimate achievable precision in parametric estimation by the measurement outcomes. The phase sensitivity [55, 56] characterizes the minimum statistical uncertainty about the estimated parameter under a given metrology protocol and hence provides a direct benchmark for comparing the precision of different metrology strategies. Theoretically, the phase sensitivity is lower bounded by the quantum Cramér-Rao bound [57] which scales inversely with the square root of QFI. When the bound is saturated, all information about the to-be-estimated parameter encoded in the probe system has

been extracted via the measurement outcomes. In addition, different measurements or detection methods applied to the same output result in different outcomes and hence phase sensitivities. Popular detection methods include homodyne detection [58, 59], intensity detection [60, 61], and parity detection [62–65]. Experimentally, parity detection can be realized in both atomic and photonic systems, through measuring the population in atomic ensembles [64] and the photon number of the cavity [65], respectively. In this section, we derive the phase sensitivity of our protocol under the parity detection.

According to the error propagation equation [66], the phase sensitivity under parity detection can be expressed as:

$$|\Delta\theta| = \frac{\sqrt{1 - \langle \Pi \rangle^2}}{|\partial \langle \Pi \rangle / \partial \theta|}, \quad (30)$$

where $\langle \Pi \rangle = \text{Tr}[\rho \Pi]$ denotes the output signal on the parity measurement Π . The following derivation is performed under the optimized settings, i.e., the optimized joint-evolution time $t_{1,\text{opt}}$, the probe eigenfrequency ω_P , and the coupling strengths of the transversal and longitudinal interactions are set by Eq. (9b) with $n_1 = 0$, Eq. (12) with $n_P = 10$, and Eq. (9a), respectively.

A. Parity detection on the ancillary qubit

We first consider the parity detection performed on the ancillary qubit with the parity operator $\Pi = \Pi_A = \sigma_z$. In the circuit model (1), after the free joint unitary evolution for Evolution 1, the parametric encoding, and the unconditional measurement, the composite system is in a separable state, with all information about the to-be-estimated parameter encoded solely in the probe system. It indicates that at this moment the parity measurement on the ancillary qubit cannot extract any information. Therefore, it is necessary to use the joint unitary evolution for Evolution 2 to transfer the encoded information from the probe system to the ancillary system. It has been shown [35, 66, 67] that such a transfer can be optimized when the joint evolution operator $U(t_2)$ becomes the time reversal of $U(t_{1,\text{opt}})$, i.e.,

$$U(t_2) = U^\dagger(t_{1,\text{opt}}) \quad (31)$$

up to a global phase. With the optimized duration t_1 in Eq. (9b), Eq. (31) is equivalent to $U(t_{1,\text{opt}})U(t_2) = e^{-iH(t_{1,\text{opt}}+t_2)} = \mathcal{I}^{2(N+1)}$. It gives rise to

$$t_2 = (4n_2 - 1)t_{1,\text{opt}} \quad (32)$$

with n_2 integer and exactly the same longitudinal coupling strength g_z in Eq. (25) by using Eqs. (9a) and (12).

With Eqs. (14), (25), and (32), one can obtain the output state of the composite system $|\Psi_{\theta,\pm}\rangle$ and hence,

$$\begin{aligned} \langle \Pi_A \rangle &= \langle \Psi_{\theta,+} | \sigma_z | \Psi_{\theta,+} \rangle + \langle \Psi_{\theta,-} | \sigma_z | \Psi_{\theta,-} \rangle \\ &= \frac{N[N^2 \cos(N\theta) + \cos\theta]}{(N+1)^2}. \end{aligned} \quad (33)$$

Then the phase sensitivity in Eq. (30) is obtained as

$$|\Delta\theta| = \frac{1}{N} \frac{\sqrt{(1+N^{-1})^4 - [\sin(N\theta) + N^{-1}\sin\theta]^2}}{|\cos(N\theta) + N^{-2}\cos\theta|}. \quad (34)$$

Its lower bound can be obtained by $d|\Delta\theta|/d\theta = 0$, which yields the optimal working points for the estimated parameter:

$$\theta_{\text{opt,A}} = k\pi \quad (35)$$

with k integer. The corresponding phase sensitivity is

$$|\Delta\theta|_{\text{min,A}} = \frac{(N+1)^2}{N(N^2+1)}. \quad (36)$$

For a large-size probe with $N \gg 1$, the phase sensitivity in Eq. (34) is approximated as $|\Delta\theta| \approx 1/N$ when $\cos\theta \neq 0$, indicating HL. In addition, by substituting $\theta = \theta_{\text{opt,A}} + \delta\theta$ with $|\delta\theta/\theta_{\text{opt,A}}| \ll 1$, the phase sensitivity around the optimal working points is

$$|\Delta\theta| \approx \frac{(N+1)^2}{N(N^2+1)} + \frac{4N+3}{2N+4} (\delta\theta)^2 \quad (37)$$

up to the second order in the phase deviation $\delta\theta$. One can find that the first order in the phase deviation $\delta\theta$ vanishes, confirming that our result about the to-be-estimated parameter $\theta_{\text{opt,A}}$ in Eq. (35) is both optimal and insensitive to the deviation of θ .

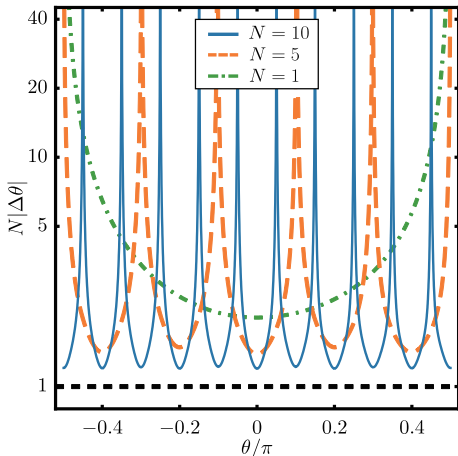


FIG. 5. Renormalized phase sensitivity $N|\Delta\theta|$ under the parity detection on the ancillary system. The black-dashed line represents HL. The probe is initialized as $|\psi\rangle = |j, -j\rangle_{\text{opt}}$ and the evolution time of Stage 2 is $t_2 = 3t_{1,\text{opt}}(n_1 = 0)$. The other parameters are the same as Fig. 3.

This result can be demonstrated by numerical evaluations of the renormalized phase sensitivity $N|\Delta\theta|$ as a function of the to-be-estimated parameter θ in Fig. 5, where the joint evolution time of the second stage t_2 is optimized by Eq. (32) with $n_2 = 1$. The horizontal line indicates the Heisenberg limit, which represents the ultimate precision achievable in phase estimation. One can

find that the phase sensitivity exhibits an almost periodic behavior with the parameter θ . The values of the phase sensitivity at the local-minimal points are nearly identical to the global-minimal point captured by Eq. (35) for a fixed probe size N . For example, when $N = 5$, we have $N|\Delta\theta| \approx 1.38, 1.48$, and 1.41 at $\theta/\pi = 0, 0.2$, and 0.4 , respectively. As the probe spin number N increases, the optimal phase sensitivity at $\theta_{\text{opt}} = 0$ approaches the Heisenberg limit (see the horizontal line). In particular, we have $N|\Delta\theta|_{\text{min,A}} \approx 2, 1.38$, and 1.20 for $N = 1, 5$, and 10 , respectively, as expected by Eq. (36). When the parameter θ deviates from the optimal working point θ_{opt} , the phase sensitivity remains close to its optimal value, e.g., we have $|\theta| \leq 0.199\pi, 0.041\pi$, and 0.021π for $N = 1, 5$, and 10 , respectively, by holding $|\Delta\theta| \leq 1.2|\Delta\theta|_{\text{min,A}}$.

B. Parity detection on the probe system

If the parity detection is performed on the probe system, then the parity operator becomes $\Pi = \Pi_P = (-1)^{j-J_z}$, by which the extractable information varies with the joint-evolution time t_2 .

In the case of $t_2 = 0$, the output state in Eq. (14) shows that the two subsystems are separable and the probe system is at a GHZ-like state. Consequently, one can obtain the output signal

$$\langle \Pi_P \rangle = \frac{N}{N+1} \sin(N\theta + j\pi + \phi), \quad (38)$$

where the parameter ϕ is given by Eq. (10). Substituting Eq. (38) to Eq. (30), we have

$$|\Delta\theta| = \frac{1}{N} \sqrt{1 + \frac{2N+1}{N^2 \cos^2(N\theta + j\pi + \phi)}}. \quad (39)$$

Similar to Sec. V A, one can obtain the minimum value of the phase sensitivity

$$|\Delta\theta|_{\text{min,P}} = \frac{N+1}{N^2}, \quad (40)$$

and the corresponding optimal working points

$$\theta_{\text{opt,P}} = \frac{1}{N} [(k_1 - j)\pi - \phi] \quad (41)$$

with k_1 integer. Despite the phase sensitivity diverges exactly at $\theta = [(k_2 - j + 1/2)\pi - \phi]/N$ with k_2 integer, it is interesting to find that the optimal working points $\theta_{\text{opt,P}}$ depend on the parameter ϕ , or more precisely, on the ratio of the coupling strength and the detuning g_z/Δ_A as indicated by Eq. (10). This result implies that, by setting different ratio g_z/Δ_A , one can shift the optimal working points $\theta_{\text{opt,P}}$ and thereby achieve an optimal metrology over the full range of the estimated phase. In addition, by substituting $\theta = \theta_{\text{opt,P}} + \delta\theta$ with $|\delta\theta/\theta_{\text{opt,P}}| \ll 1$, the phase sensitivity in Eq. (39) can be written as

$$|\Delta\theta| \approx \frac{N+1}{N^2} + \frac{2N+1}{2N+2} (\delta\theta)^2 \quad (42)$$

up to the second order of the phase deviation $\delta\theta$. It confirms that our result about the to-be-estimated parameter $\theta_{\text{opt},P}$ in Eq. (41) is optimal.

In the case of $t_2 \neq 0$, the probe system becomes entangled again with the ancillary qubit, causing the information about the estimated parameter to be distributed across the two subsystems. An effective approach to enhance the ultimate precision is to drive the composite system back to a separable state, i.e., $U(t_2) = \mathcal{I}^{2(N+1)}$. Consequently, one can find the longitudinal coupling strength is that given by Eq. (25) and the exact solution of the evolution time is

$$t_2 = 4n_3 t_{1,\text{opt}} \quad (43)$$

with n_3 nonzero integer, where the optimized joint evolution time $t_{1,\text{opt}}$ is given by Eq. (9b). Using Eqs. (14), (25), and (43), the output signal becomes

$$\langle \Pi_P \rangle = \frac{N}{N+1} \cos(N\theta + j\pi). \quad (44)$$

Substituting Eq. (44) to Eq. (30), we have the phase sensitivity

$$|\Delta\theta| = \frac{1}{N} \sqrt{1 + \frac{2N+1}{N^2 \sin^2(N\theta + j\pi)}}. \quad (45)$$

One can find that the result in Eq. (45) is exactly the same as Eq. (39) with $\phi = \pi/2$. Thus, one can locate the minimum value of the phase sensitivity in Eq. (40) and the optimal working points $\theta_{\text{opt},P} = [2k_1 - (N+1)]\pi/(2N)$ according to Eq. (41).

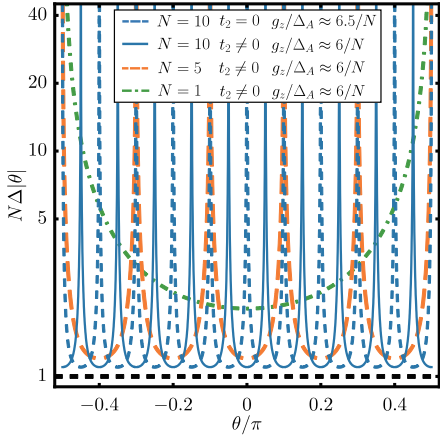


FIG. 6. Renormalized phase sensitivity $N|\Delta\theta|$ under the parity detection on the probe system with various N . The black-dashed line indicates the Heisenberg limit. The probe-spin ensemble is initialized as $|\psi\rangle = |j, -j\rangle_{\text{opt}}$ and the evolution time of Stage 2 is set as $t_2 = 0$ or $t_2 = 4t_{1,\text{opt}}(n_1 = 0)$. The other parameters are the same as Fig. 3.

The complementarity of $t_2 = 0$ and $t_2 \neq 0$ can be found in Fig. 6, that demonstrates the phase sensitivity about

θ under the parity detection on the probe system. As indicated by the blue-solid line and the blue-dashed line, the phase estimation over the whole regime can be optimized provided that one set two slightly different longitudinal coupling strength g_z . The green dot-dashed line, the yellow dashed line, and the blue solid line are used to show the dependence of the renormalized phase sensitivity on the probe size N with $t_2 = 4t_{1,\text{opt}}(n_1 = 0)$. Different from Fig. 5, the local local-minimal points of the phase sensitivity are also the global-minimal points as suggested by Eq. (41). For example, when $N = 5$, we have $N|\Delta\theta| = 1.2$ at $\theta/\pi = 0, \pm 0.2$, and ± 0.4 . As the probe size N increases, the phase sensitivity at the optimal working points $\theta_{\text{opt},P}$ approaches HL. In particular, we have $N|\Delta\theta|_{\text{min},P} = 2, 1.2$, and 1.1 for $N = 1, 5$, and 10 , respectively. In comparison to Fig. 5, the last two results are lower than that obtained by the parity detection on the ancillary qubit. More important for the parity detection on the probe system, we find a wider regime about θ over which the phase sensitivity remains nearby its optimal value. To hold $|\Delta\theta| \leq 1.2|\Delta\theta|_{\text{min},P}$, we have $|\theta| \leq 0.208\pi, 0.056\pi$, and 0.032π for $N = 1, 5$, and 10 , respectively.

VI. CONCLUSION

In summary, we incorporate the unconditional measurement on ancillary qubit to the phase estimation over a probe spin ensemble. The two components are weakly coupled to each other via a general Heisenberg XXZ interaction. It is a metrology protocol for large-spin systems without GHZ-like state, nonlinear Hamiltonian, and strong or tunable external coupling strength. In our measurement-based metrology protocol, either polarized state or thermal state with a large probe size N can be used to achieve an exact or asymptotic Heisenberg-scaling behavior N^2 in parameter estimation. We show that this quadratic scaling behavior is insensitive to the precise controls over the direction of the phase encoding and the coupling strengths. To achieve the ultimate precision, we propose to minimize the phase sensitivity through the parity detection on either the probe system or the ancillary qubit. It turns out that in both schemes, the phase sensitivity can approach the Heisenberg limit at the optimal working points. Under certain conditions, one can achieve optimal metrology precision over the entire regime of the to-be-estimated phase. In essence, our work paves an economical way toward the Heisenberg-scaling metrology.

ACKNOWLEDGMENTS

We acknowledge grant support from the National Natural Science Foundation of China (Grant No. U25A20199) and the “Pioneer” and “Leading Goose” R&D of Zhejiang Province (Grant No. 2025C01028).

Appendix A: Time evolution operator for the XXZ Hamiltonian

This appendix contributes to deriving the unitary evolution operator for the full Hamiltonian in Eq. (1), which is recalled as

$$\begin{aligned} H &= H_0 + H_I, \\ H_0 &= \omega_P J_z + \omega_A \sigma_z, \\ H_I &= g_z J_z \sigma_z + g(J_x \sigma_x + J_y \sigma_y). \end{aligned} \quad (\text{A1})$$

Due to the commutation relation $[H_0, H_I] = 0$, the time evolution operator for H can be partitioned into the subspaces $|j, j, e\rangle \oplus |j, -j, g\rangle \oplus \{|j, m+1, g\rangle, |j, m, e\rangle\}$ with $-j \leq m \leq j-1$ for quantum number $j = N/2$. N is the size of the probe spin ensemble. The Hamiltonian in a typical subspace $\{|j, m+1, g\rangle, |j, m, e\rangle\}$ can be written as

$$H_m = \left(m + \frac{1}{2}\right) \omega_P - \frac{1}{2} g_z + \begin{pmatrix} -\Lambda_m & \omega_m \\ \omega_m & \Lambda_m \end{pmatrix}, \quad (\text{A2})$$

with $\omega_m = g\sqrt{(j-m)(j+m+1)}$, $\Lambda_m = (m+1/2)g_z + \Delta_A$, and $\Delta_A \equiv \omega_A - \omega_P/2$. The evolution operator in the relevant subspace thus reads

$$e^{-iH_m t} = e^{-i[(m+1/2)\omega_P - g_z/2]t} \times \begin{pmatrix} \cos(\Omega_m t) + \frac{i\Lambda_m}{\Omega_m} \sin(\Omega_m t) & -\frac{i\omega_m}{\Omega_m} \sin(\Omega_m t) \\ -\frac{i\omega_m}{\Omega_m} \sin(\Omega_m t) & \cos(\Omega_m t) - \frac{i\Lambda_m}{\Omega_m} \sin(\Omega_m t) \end{pmatrix}, \quad (\text{A3})$$

with $\Omega_m = \sqrt{\Lambda_m^2 + \omega_m^2}$.

Consequently, the time evolution operator in the whole

Hilbert space can be organized as

$$\begin{aligned} e^{-iHt} &= \sum_{m=-j}^{j-1} e^{-iH_m t} + e^{-i[j(\omega_P + g_z) + \omega_A]t} |j, j, e\rangle \langle j, j, e| \\ &\quad + e^{i[j(\omega_P - g_z) + \omega_A]t} |j, -j, g\rangle \langle j, -j, g|. \end{aligned} \quad (\text{A4})$$

Using the functions of the operator J_z , the full evolution operator can be rewritten in a more explicit way:

$$\begin{aligned} e^{-iHt} &= \left\{ \left[\cos \Omega(J_z) t - \frac{i\Lambda(J_z)}{\Omega(J_z)} \sin \Omega(J_z) t \right] \otimes |e\rangle \langle e| \right. \\ &\quad - ie^{i\omega_P t} g \frac{\sin \Omega(J_z) t}{\Omega(J_z)} J_- \otimes |e\rangle \langle g| \\ &\quad - ig J_+ \frac{\sin \Omega(J_z) t}{\Omega(J_z)} \otimes |g\rangle \langle e| \\ &\quad + \left[\cos \Omega(J_z - 1) t + \frac{i\Lambda(J_z - 1)}{\Omega(J_z - 1)} \sin \Omega(J_z - 1) t \right] \\ &\quad \left. \otimes |g\rangle \langle g| e^{i\omega_P t} \right\} e^{-iA(J_z)t}, \end{aligned} \quad (\text{A5})$$

where

$$\omega(J_z) \equiv g\sqrt{(j - J_z)(j + J_z + 1)}. \quad (\text{A6a})$$

$$\Lambda(J_z) \equiv g_z \left(J_z + \frac{1}{2}\right) + \Delta_A, \quad (\text{A6b})$$

$$\Omega(J_z) \equiv \sqrt{\omega^2(J_z) + \Lambda^2(J_z)}. \quad (\text{A6c})$$

$$A(J_z) \equiv \omega_P \left(J_z + \frac{1}{2}\right) - \frac{g_z}{2}, \quad (\text{A6d})$$

as given in Eqs. (7a), (7b), (7c), and (7d) in the main text.

[1] Z. Sun, J. Ma, X.-M. Lu, and X.-G. Wang, *Fisher information in a quantum-critical environment*, *Phys. Rev. A* **82**, 022306 (2010).

[2] J. Ma, Y.-X. Huang, X.-G. Wang, and C. P. Sun, *Quantum fisher information of the greenberger-horne-zeilinger state in decoherence channels*, *Phys. Rev. A* **84**, 022302 (2011).

[3] M. G. Genoni, S. Olivares, D. Brivio, S. Cialdi, D. Cipriani, A. Santamato, S. Vezzoli, and M. G. A. Paris, *Optical interferometry in the presence of large phase diffusion*, *Phys. Rev. A* **85**, 043817 (2012).

[4] B. M. Escher, L. Davidovich, N. Zagury, and R. L. de Matos Filho, *Quantum metrological limits via a variational approach*, *Phys. Rev. Lett.* **109**, 190404 (2012).

[5] W. Zhong, Z. Sun, J. Ma, X. Wang, and F. Nori, *Fisher information under decoherence in bloch representation*, *Phys. Rev. A* **87**, 022337 (2013).

[6] V. Giovannetti, S. Lloyd, and L. Maccone, *Quantum-enhanced measurements: beating the standard quantum limit*, *Science* **306**, 1330 (2004).

[7] A. D. Ludlow, M. M. Boyd, J. Ye, E. Peik, and P. O. Schmidt, *Optical atomic clocks*, *Rev. Mod. Phys.* **87**, 637 (2015).

[8] H. Katori, *Optical lattice clocks and quantum metrology*, *Nat. Photon.* **5**, 203 (2011).

[9] C. M. Caves, *Quantum-mechanical noise in an interferometer*, *Phys. Rev. D* **23**, 1693 (1981).

[10] M. A. Taylor and W. P. Bowen, *Quantum metrology and its application in biology*, *Phys. Rep.* **615**, 1 (2016).

[11] N. Mauranyapin, L. Madsen, M. Taylor, M. Waleed, and W. Bowen, *Evanescence single-molecule biosensing with quantum-limited precision*, *Nat. Photon.* **11**, 477 (2017).

[12] J. A. Jones, S. D. Karlen, J. Fitzsimons, A. Ardavan, S. C. Benjamin, G. A. D. Briggs, and J. J. Morton, *Magnetic field sensing beyond the standard quantum limit using 10-spin noon states*, *Science* **324**, 1166 (2009).

[13] S. M. Kay, *Fundamentals of statistical signal processing: estimation theory* (Prentice-Hall, Inc., 1993).

[14] V. Giovannetti, S. Lloyd, and L. Maccone, *Quantum metrology*, *Phys. Rev. Lett.* **96**, 010401 (2006).

[15] C. Song, K. Xu, H.-K. Li, Y.-R. Zhang, X. Zhang, W.-X. Liu, Q.-J. Guo, Z. Wang, W.-H. Ren, J. Hao, *et al.*, *Generation of multicomponent atomic schrödinger cat states of up to 20 qubits*, *Science* **365**, 574 (2019).

[16] T. Chalopin, C. Bouazza, A. Evrard, V. Makhalov, D. Dreon, J. Dalibard, L. A. Sidorenkov, and S. Nascimbene, *Quantum-enhanced sensing using non-classical spin states of a highly magnetic atom*, *Nat. Commun.* **9**, 4955 (2018).

[17] H. Kaufmann, T. Ruster, C. T. Schmiegelow, M. A. Luda, V. Kaushal, J. Schulz, D. Von Lindenfels, F. Schmidt-Kaler, and U. Poschinger, *Scalable creation of long-lived multipartite entanglement*, *Phys. Rev. Lett.* **119**, 150503 (2017).

[18] M. Kitagawa and M. Ueda, *Squeezed spin states*, *Phys. Rev. A* **47**, 5138 (1993).

[19] D. J. Wineland, J. J. Bollinger, W. M. Itano, and D. J. Heinzen, *Squeezed atomic states and projection noise in spectroscopy*, *Phys. Rev. A* **50**, 67 (1994).

[20] Y.-M. Zhang, X.-W. Li, W. Yang, and G.-R. Jin, *Quantum fisher information of entangled coherent states in the presence of photon loss*, *Phys. Rev. A* **88**, 043832 (2013).

[21] D. J. Wineland, J. J. Bollinger, W. M. Itano, F. L. Moore, and D. J. Heinzen, *Spin squeezing and reduced quantum noise in spectroscopy*, *Phys. Rev. A* **46**, R6797 (1992).

[22] A. Sørensen, L.-M. Duan, J. I. Cirac, and P. Zoller, *Many-particle entanglement with bose-einstein condensates*, *Nature* **409**, 63 (2001).

[23] C. Gross, T. Zibold, E. Nicklas, J. Esteve, and M. K. Oberthaler, *Nonlinear atom interferometer surpasses classical precision limit*, *Nature* **464**, 1165 (2010).

[24] M. F. Riedel, P. Böhi, Y. Li, T. W. Hänsch, A. Sinatra, and P. Treutlein, *Atom-chip-based generation of entanglement for quantum metrology*, *Nature* **464**, 1170 (2010).

[25] M. H. Schleier-Smith, I. D. Leroux, and V. Vuletić, *Squeezing the collective spin of a dilute atomic ensemble by cavity feedback*, *Phys. Rev. A* **81**, 021804 (2010).

[26] I. D. Leroux, M. H. Schleier-Smith, and V. Vuletić, *Implementation of cavity squeezing of a collective atomic spin*, *Phys. Rev. Lett.* **104**, 073602 (2010).

[27] M. A. Norcia, R. J. Lewis-Swan, J. R. Cline, B. Zhu, A. M. Rey, and J. K. Thompson, *Cavity-mediated collective spin-exchange interactions in a strontium superradiant laser*, *Science* **361**, 259 (2018).

[28] K. Mølmer and A. Sørensen, *Multiparticle entanglement of hot trapped ions*, *Phys. Rev. Lett.* **82**, 1835 (1999).

[29] J. W. Britton, B. C. Sawyer, A. C. Keith, C.-C. J. Wang, J. K. Freericks, H. Uys, M. J. Biercuk, and J. J. Bollinger, *Engineered two-dimensional ising interactions in a trapped-ion quantum simulator with hundreds of spins*, *Nature* **484**, 489 (2012).

[30] J. G. Bohnet, B. C. Sawyer, J. W. Britton, M. L. Wall, A. M. Rey, M. Foss-Feig, and J. J. Bollinger, *Quantum spin dynamics and entanglement generation with hundreds of trapped ions*, *Science* **352**, 1297 (2016).

[31] A. Sørensen and K. Mølmer, *Spin-spin interaction and spin squeezing in an optical lattice*, *Phys. Rev. Lett.* **83**, 2274 (1999).

[32] P. He, M. A. Perlin, S. R. Muleady, R. J. Lewis-Swan, R. B. Hutson, J. Ye, and A. M. Rey, *Engineering spin squeezing in a 3d optical lattice with interacting spin-orbit-coupled fermions*, *Phys. Rev. Res.* **1**, 033075 (2019).

[33] T. Hernández Yanes, M. Płodzień, M. Macko, Sinkevičienė, G. Žlabys, G. Juzeliūnas, and E. Witkowska, *One-and two-axis squeezing via laser coupling in an atomic fermi-hubbard model*, *Phys. Rev. Lett.* **129**, 090403 (2022).

[34] J. Fan and S. Pang, *Achieving heisenberg scaling by probe-ancilla interaction in quantum metrology*, *Phys. Rev. A* **110**, 062406 (2024).

[35] P. Chen and J. Jing, *Qubit-assisted quantum metrology under a time-reversal strategy*, *Phys. Rev. A* **110**, 062425 (2024).

[36] D.-W. Luo and T. Yu, *Time-reversal assisted quantum metrology with an optimal control*, *arXiv:2312.14443* (2023).

[37] S. Boixo, S. T. Flammia, C. M. Caves, and M. Geremia, *Generalized limits for single-parameter quantum estimation*, *Phys. Rev. Lett.* **98**, 090401 (2007).

[38] R. Demkowicz-Dobrzański and L. Maccone, *Using entanglement against noise in quantum metrology*, *Phys. Rev. Lett.* **113**, 250801 (2014).

[39] J. Yang, S. Pang, Z. Chen, A. N. Jordan, and A. Del Campo, *Variational principle for optimal quantum controls in quantum metrology*, *Phys. Rev. Lett.* **128**, 160505 (2022).

[40] C. S. Kumar and T. Mahesh, *Ancilla-induced amplification of quantum fisher information*, *Eur. Phys. J. Plus* **133**, 460 (2018).

[41] W.-T. He, H.-Y. Guang, Z.-Y. Li, R.-Q. Deng, N.-N. Zhang, J.-X. Zhao, F.-G. Deng, and Q. Ai, *Quantum metrology with one auxiliary particle in a correlated bath and its quantum simulation*, *Phys. Rev. A* **104**, 062429 (2021).

[42] B. Xia, J. Huang, H. Li, Z. Luo, and G. Zeng, *Nanoradian-scale precision in light rotation measurement via indefinite quantum dynamics*, *Sci. Adv.* **10**, eadm8524 (2024).

[43] J. F. Barry, J. M. Schloss, E. Bauch, M. J. Turner, C. A. Hart, L. M. Pham, and R. L. Walsworth, *Sensitivity optimization for nv-diamond magnetometry*, *Rev. Mod. Phys.* **92**, 015004 (2020).

[44] X.-F. He, N. B. Manson, and P. T. Fisk, *Paramagnetic resonance of photoexcited n-v defects in diamond. ii. hyperfine interaction with the n 14 nucleus*, *Physical Review B* **47**, 8816 (1993).

[45] W. Yao, R.-B. Liu, and L. J. Sham, *Theory of electron spin decoherence by interacting nuclear spins in a quantum dot*, *Phys. Rev. B* **74**, 195301 (2006).

[46] R.-B. Liu, W. Yao, and L. Sham, *Control of electron spin decoherence caused by electron-nuclear spin dynamics in a quantum dot*, *New J. Phys.* **9**, 226 (2007).

[47] V. Meyer, M. A. Rowe, D. Kielpinski, C. A. Sackett, W. M. Itano, C. Monroe, and D. J. Wineland, *Experimental demonstration of entanglement-enhanced rotation angle estimation using trapped ions*, *Phys. Rev. Lett.* **86**, 5870 (2001).

[48] C. F. Ockeloen, R. Schmied, M. F. Riedel, and P. Treutlein, *Quantum metrology with a scanning probe atom interferometer*, *Phys. Rev. Lett.* **111**, 143001 (2013).

[49] T. Xie, Z. Zhao, X. Kong, W. Ma, M. Wang, X. Ye, P. Yu, Z. Yang, S. Xu, P. Wang, *et al.*, *Beating the standard quantum limit under ambient conditions with solid-state spins*, *Sci. Adv.* **7**, eabg9204 (2021).

[50] S. Pang and T. A. Brun, *Quantum metrology for a general hamiltonian parameter*, *Phys. Rev. A* **90**, 022117 (2014).

[51] X. Zhao, Y. Yang, and G. Chiribella, *Quantum metrology with indefinite causal order*, *Phys. Rev. Lett.* **124**, 190503 (2020).

[52] P. Yin, X. Zhao, Y. Yang, Y. Guo, W.-H. Zhang, G.-C. Li, Y.-J. Han, B.-H. Liu, J.-S. Xu, G. Chiribella, *et al.*, *Experimental super-heisenberg quantum metrology with indefinite gate order*, *Nat. Phys.* **19**, 1122 (2023).

[53] B. Xia, J. Huang, H. Li, Z. Luo, and G. Zeng, *Nanoradian-scale precision in light rotation measurement via indefinite quantum dynamics*, *Sci. Adv.* **10**, eadm8524 (2024).

[54] S. L. Braunstein and C. M. Caves, *Statistical distance and the geometry of quantum states*, *Phys. Rev. Lett.* **72**, 3439 (1994).

[55] R. Demkowicz-Dobrzański, M. Jarzyna, and J. Kołodyński, *Quantum limits in optical interferometry*, *Prog. Opt.* **60**, 345 (2015).

[56] M. Bradshaw, P. K. Lam, and S. M. Assad, *Ultimate precision of joint quadrature parameter estimation with a gaussian probe*, *Phys. Rev. A* **97**, 012106 (2018).

[57] C. W. Helstrom, *Quantum detection and estimation theory*, *J. Stat. Phys.* **1**, 231 (1969).

[58] H. P. Yuen and V. W. Chan, *Noise in homodyne and heterodyne detection*, *Opt. lett.* **8**, 177 (1983).

[59] M. Manceau, F. Khalili, and M. Chekhova, *Improving the phase super-sensitivity of squeezing-assisted interferometers by squeeze factor unbalancing*, *New J. Phys.* **19**, 013014 (2017).

[60] S. S. Szigeti, R. J. Lewis-Swan, and S. A. Haine, *Pumped-up $su(1,1)$ interferometry*, *Phys. Rev. Lett.* **118**, 150401 (2017).

[61] S. Ataman, A. Preda, and R. Ionicioiu, *Phase sensitivity of a mach-zehnder interferometer with single-intensity and difference-intensity detection*, *Phys. Rev. A* **98**, 043856 (2018).

[62] J. J. Bollinger, W. M. Itano, D. J. Wineland, and D. J. Heinzen, *Optimal frequency measurements with maximally correlated states*, *Phys. Rev. A* **54**, R4649 (1996).

[63] P. M. Anisimov, G. M. Raterman, A. Chiruvelli, W. N. Plick, S. D. Huver, H. Lee, and J. P. Dowling, *Quantum metrology with two-mode squeezed vacuum: Parity detection beats the heisenberg limit*, *Phys. Rev. Lett.* **104**, 103602 (2010).

[64] T. Kielinski, P. O. Schmidt, and K. Hammerer, *Ghz protocols enhance frequency metrology despite spontaneous decay*, *Sci. Adv.* **10**, eadr1439 (2024).

[65] X. Deng, S. Li, Z.-J. Chen, Z. Ni, Y. Cai, J. Mai, L. Zhang, P. Zheng, H. Yu, C.-L. Zou, *et al.*, *Quantum-enhanced metrology with large fock states*, *Nat. Phys.* **20**, 1874 (2024).

[66] B. Yurke, S. L. McCall, and J. R. Klauder, *$Su(2)$ and $su(1,1)$ interferometers*, *Phys. Rev. A* **33**, 4033 (1986).

[67] L. Pezzè, M. A. Ciampini, N. Spagnolo, P. C. Humphreys, A. Datta, I. A. Walmsley, M. Barbieri, F. Sciarrino, and A. Smerzi, *Optimal measurements for simultaneous quantum estimation of multiple phases*, *Phys. Rev. Lett.* **119**, 130504 (2017).